BBA - General Subjects 1863 (2019) 565–576

Contents lists available at ScienceDirect

BBA - General Subjects

journal homepage: www.elsevier.com/locate/bbagen

Structure-based design and application of an engineered glutathione transferase for the development of an optical biosensor for pesticides determination

Evangelia G. Chronopoulou[a], Dimitrios Vlachakis[b], Anastassios C. Papageorgiou[c], Farid S. Ataya[d], Nikolaos E. Labrou[a,*]

[a] Laboratory of Enzyme Technology, Department of Agricultural Biotechnology, Agricultural University of Athens, 75 Iera Odos Street, GR-11855 Athens, Greece
[b] Laboratory of Genetics, Department of Biotechnology, School of Food, Biotechnology and Development, Agricultural University of Athens, 75 Iera Odos Street, GR-11855 Athens, Greece
[c] Turku Centre for Biotechnology, University of Turku, Åbo Akademi University, Turku 20521, Finland
[d] Department of Biochemistry, College of Science, King Saud University, P.O. Box 2455, Riyadh 11451, Saudi Arabia

ARTICLE INFO

Keywords:
Glutathione transferase
Protein engineering
Biosensor
Pesticides determination
α-Endosulfan

ABSTRACT

In the present work, a structure-based design approach was used for the generation of a novel variant of synthetic glutathione transferase (*PvGm*GSTU) with higher sensitivity towards pesticides. Molecular modelling studies revealed Phe117 as a key residue that contributes to the formation of the hydrophobic binding site (H-site) and modulates the affinity of the enzyme towards xenobiotic compounds. Site-saturation mutagenesis of position Phe117 created a library of *PvGm*GSTU variants with altered kinetic and binding properties. Screening of the library against twenty-five different pesticides, showed that the mutant enzyme Phe117Ile displays 3-fold higher catalytic efficiency and exhibits increased affinity towards α-endosulfan, compared to the wild-type enzyme. Based on these catalytic features the mutant enzyme Phe117Ile was explored for the development of an optical biosensor for α-endosulfan. The enzyme was entrapped in alkosixylane sol-gel system in the presence of two pH indicators (bromocresol purple and phenol red). The sensing signal was based on the inhibition of the sol-gel entrapped GST, with subsequent decrease of released [H^+] by the catalytic reaction, measured by sol–gel entrapped indicators. The assay response at 562 nm was linear in the range pH = 4–7. Linear calibration curves were obtained for α-endosulfan in the range of 0–30 μM. The reproducibility of the assay response, expressed by relative standard deviation, was in the order of 4.1% (N = 28). The method was successfully applied to the determination of α-endosulfan in real water samples without sample preparation steps.

1. Introduction

Over the last three decades there has been an intense research interest in the field of enzyme biosensors. These analytical tools, except of being accurate, environmentally benign and safe, they can provide real-time monitoring with minimum sample preparation in a simple and efficient manner [1–5]. Enzymatic biosensing methods based on enzyme activity or inhibition have been widely used [6]. Some examples include the enzymes cholinesterases, organophosphate hydrolase, alkaline and acid phosphatase, ascorbate oxidase, lipase etc. [7,8].

In enzyme-based biosensors the enzymes are immobilized by adsorption, cross-linking, covalent bond formation, entrapment or affinity capture [5,9,10]. In the entrapment method, the enzyme is restricted within a three-dimensional structure of a matrix such as silicate materials using the sol-gel process, electropolymerized films, polysaccharide or carbon paste [5,11,12]. This method provides simplicity and stabilization of enzyme activity. However, leaching of enzyme and possible diffusion barriers are the main disadvantages [5]. The sol-gel process involves hydrolysis of alkoxide precursors under acidic conditions followed by condensation of the hydroxylated units, which leads to the formation of a porous gel [5,11–13]. The alkoxide precursor molecules are hydrolyzed in the presence of water at low pH, resulting

Abbreviations: ANNs, Artificial Neural Networks; G-site, glutathione-binding site; GSH, glutathione; GST, glutathione transferase; H-site, hydrophobic-binding site; MD, molecular dynamics; PTMOS, phenyltrimethoxysilane; TEOS, tetraethyl orthosilicate; PEG, polyethylene glycol; *PvGm*GSTUG, Synthetic glutathione transferase from *Phaseolus vulgaris* and *Glycine* max; RDS, relative standard deviation

* Corresponding author.
E-mail address: lambrou@aua.gr (N.E. Labrou).

https://doi.org/10.1016/j.bbagen.2018.12.004
Received 30 July 2018; Received in revised form 8 November 2018; Accepted 4 December 2018
Available online 24 December 2018
0304-4165/

in the formation of silanol (Si—OH) groups. In the second step, the condensation reaction between silanol moieties at alkaline (or acidic) pH results in the formation of siloxane (Si—O—Si) polymers, generating a matrix in which an enzyme can be entrapped [14,15].

Glutathione transferases (GSTs, EC 2.5.1.18) comprise a family of enzymes that are involved in the detoxification mechanism of endogenous and xenobiotic electrophile compounds [16–20]. They catalyze the nucleophilic attack of reduced glutathione (GSH) on the electrophilic centre of xenobiotic compounds [21]. Different GST isoenzymes have already found successful applications in the development of enzyme biosensors for the determination of herbicides and insecticides [3,9,17,22–26].

Enzyme engineering is the process of improving the catalytic, functional or structural features of an enzyme by modifying its amino acid sequence [27]. The goal of this technology is to improve or overcome the potential disadvantages of native enzymes (e.g. low stability, low specificity and catalytic activity), aiming at maximizing the biocatalytic applications of the enzymes [28]. A number of interesting engineering studies can be found in the literature [29–32]. Rational design using computational tools and directed evolution are the two main approaches in enzyme engineering [33–35]. However, the combination of directed evolution and rational protein design is becoming increasingly useful and effective [36]. The application of enzyme engineering for the development of tailor-made enzymes with improved properties for application in biosensor technology is gaining particular interest over the last years [28]. Enzyme mutants with higher sensitivity can improve biosensor's analytical performance such as durability and sensitivity [8,24].

The present work, through the combination of directed evolution and rational protein design approach, aims at the development of an optimized GST mutant for the creation of an optical GST-based biosensor for α-endosulfan. Endosulfan is a toxic insecticide which is considered as a major Persistent Organic Pollutant (POP). It has been detected in a variety of environmental samples across the world [37]. The development, therefore, of a new method for direct determination of endosulfan in environmental samples (e.g. water) has both scientific interest and practical importance.

2. Materials and methods

2.1. Materials

All enzyme substrates, antibiotics, tetraethyl orthosilicate (TEOS), phenyltrimethoxysilane (PTMOS) and polyethylene glycol (PEG) were purchased from Sigma-Aldrich, (USA). Ampicillin and chloramphenicol were purchased from Sigma-Aldrich, (USA). KAPA Taq and KAPA High fidelity DNA polymerases were purchased from KAPA Biosystems (USA). Plasmid purification kit was obtained by Macherey–Nagel, (Germany) and QIAquickTM Gel Extraction kit from Quiage (Germany). The pesticides: fenvalerate, permethrin, diazinon, malathion, carbaryl, atrazine, diuron, fluorodifen, alachlor, metolachlor, dichlorvos, omethoate, λ-cypermethrin, dieldrin, spirodiclofen, α-cyhalothrin, spinosad, deltamethrin, aldrin, spiromesifen, thiacloprid, pirimicarb, methomyl, chlorpyriphos, endosulfan, carbofuran and fluazifop-p-butyl were purchased from Riedel de Haen (Germany).

3. Methods

3.1. Protein determination

Protein concentration was determined by the Bradford assay using BSA (fraction V) as a standard [38].

3.2. Site-saturation mutagenesis

The expression construct pT7*PvGm*GSTUG [39] was used as template for site-saturation mutagenesis at amino acid position 117, using the quick-change method [23]. The mutations were introduced using a set of degenerate synthetic oligonucleotides, in which the mutation site was diversified using a randomized NNN codon. The pairs of oligonucleotide primers used in the PCR reactions for the saturation mutagenesis were as follows:

FPrimer117 5′ AAA GCT ACT NNN TCT ATT GAT 3′

RPrimer117 5′ ATC AAT AGA NNN AGT AGC TTT 3′

The PCR contained: 8 pmol of each primer, 5× Kapa High Fidelity DNA polymerase's buffer, 100 μM each dNTP, 5 ng of plasmid DNA-shuffling and 1 U Kapa HiFi DNA polymerase. The PCR comprised of 30 cycles of denaturation at 94 °C for 2 min, annealing at 40 °C for 2 min and polymerization at 72 °C for 2 min. A final extension time at 72 °C for 10 min was performed, after the 30th cycle. After completion of the PCR, the reaction product was subjected to *Dpn*I digestion. Following digestion, the mutated plasmids DNA (pEXP5-CT/TOPO/TA) were used to transform competent *E. coli* TOP10 cells. Transformed cells were selected by LB agar plate containing ampicillin (100 μg/mL). The site-saturation library was screened by measuring the enzyme activities-using CDNB/GSH substrate system. Transformants were grown at 37 °C in LB medium (10 mL) containing ampicillin (100 μg/mL).

3.3. Expression and purification of the wild-type and mutants' enzymes

E. coli cells (BL21(DE3) or BL21(DE3)pLysS), harbouring the recombinant plasmid pT7*PvGm*GSTUG were grown at 37 °C in LB medium containing ampicillin (100 μg/mL) and chloramphenicol (34 μg/mL) (for the BL21(DE3)pLysS strain). Protein expression was performed as described by Chronopoulou et al. [39]. Enzyme purification was carried out using affinity chromatography as described by Chronopoulou et al. [39]. Protein purity was judged by SDS PAGE.

3.4. Assay of enzyme activity and kinetic analysis

GST assays were performed by measuring the reaction rate (37 °C) between CDNB (1 mM) and GSH (2.5 mM) at 340 nm ($\varepsilon = 9.6\,mM^{-1}\cdot cm^{-1}$) as previously described [17]. Steady-state kinetic analysis were carried out as described by Chronopoulou et al. [17]. Curve-fits were obtained using the GrafPad (GraphPad Software Inc., Version 7.00) computer program.

3.5. Inhibition analysis and screening of the wild type and mutants *PvGmGSTUGs*

GST inhibition analysis was performed using the CDNB/GSH system, as described above, in the presence or absence of 100 μM pesticide diluted in acetone. During the course of the assay (30–60 s) no measurable pesticide/GSH conjugation was observed. The IC_{50} values of α-endosulfan were measured using the CDNB/GSH assay system in the presence of different concentrations of α-endosulfan (0–100 μM), respectively. The IC_{50} values were determined by fitting the concentration–response data to the following Eq. (2):

$$\%\text{inhibition} = \frac{100}{1 + (IC_{50}/[I])} \quad (2)$$

where [I] is the pesticide concentration. The IC_{50} values were determined using the program GraphPad Prism version 7.00.

3.6. Biocomputing analysis

3.6.1. Sequence database search and phylogenetic tree construction

In order to identify homologous *PvGm*GSTUG protein sequences, the non-redundant publicly available databases: UniProtKB [40] and GenBank [41] were searched with the entire amino acid sequences of *PvGm*GSTUG applying reciprocal BLASTp and tBLASTn [42]. The entire *PvGm*GSTUG amino acid sequence was searched against PROSITE [43],

in order to identify protein domains. The retrieved protein sequences were aligned using CLUSTALW [44]. The resulting multiple sequence alignment was trimmed by applying Gblocks [45] with default options, and subsequently was used to reconstruct a phylogenetic tree by employing the neighbor-joining method [46]. The number of amino acid substitutions per site was estimated using the JTT model [47].

3.6.2. Molecular docking

To in silico establish the complex structures of the *PvGm*GSTUG and α-endosulfan or GSH, the docking suite ZDOCK (version 3.0) was used [48]. Docking experiments were conducted on the models that had been energetically minimized and conformationally optimized using molecular dynamics simulations. ZDOCK uses a scoring function that returns electrostatic, hydrophobic and desolvation energies as well as performing a fast pairwise shape complementarity evaluation. RDOCK was utilized to refine and quickly evaluate the results obtained by ZDOCK [48]. RDOCK performs a fast minimization step to the ZDOCK molecular complex outputs and re-ranks them according to their re-calculated binding free energies.

3.6.3. Energy minimization and molecular dynamics simulations

Energy minimizations were used to remove any residual geometrical strain in each molecular system, using the Charmm27 forcefield as it is implemented into the Gromacs suite, version 4.5.5 [49]. All Gromacs-related simulations were performed though our previously developed graphical interface [50]. Molecular systems were then subjected to unrestrained Molecular Dynamics Simulations (MDS) using the Gromacs suite, version 4.5.5 [49]. MDS took place in a SPC water-solvated, periodic environment. Water molecules were added using the truncated octahedron box extending 7 Å from each atom. Molecular systems were neutralized with counter-ions as required. For the purposes of this study all MDS were performed using the NVT ensemble in a canonical environment, at 300 K and a step size equal to 2 femtoseconds for a total 100 ns simulation time. An NVT ensemble requires that the Number of atoms, Volume and Temperature remain constant throughout the simulation.

3.7. Entrapment of enzyme and pH indicators in sol-gel

Sol–gel formation was carried out as previously described [9]. The hybrid sol-gel contained TEOS and PTMOS in a 2:1 M ratio. In a glass vial, TEOS (1.10 mL), PTMOS (0.45 mL), CTAB (82 mM), ethanol (0.50 mL), water (0.70 mL) and 0.1 M HCl (0.35 mL), were added. The vial was capped and placed in an ultrasonic bath for 10 min. After sonication, the clear solution was left at room temperature, for approximately 15 h. One mL of the sol-gel was withdrawn and added to a vial containing 3.0 mg of bromocresol purple and phenol red (1:1 ratio) indicator. Then, 20 μL of the mixture were placed on a microscope slide and left at 4 °C for 24 h. The same procedure was followed for enzyme by keeping the sol-gel mixture for 1 h at 4 °C. The enzyme (0.95–2.4 U/mL) was mixed with polyethylene glycol N-hydroxy-hydroxysuccinimide ester (1:1 w/v) and left for 1 h at the same temperature, before mixing. Then, the mixture (200–500 μL) was placed in a glass cuvette and 30–60 μL KOH (1 M) was added for xerogel formation. "Aging" of xerogel was achieved using TEOS (2 or 5 days). The sol-gel was stored in potassium phosphate buffer (1 mM, pH = 7).

3.8. Determination of α-endosulfan in natural water samples

Recovery experiments were carried out using drinking water (collected from Athens water supply network) and mineral water samples (Korpi, NESTLE Hellas), spiked with known amounts (0.8–16 μM) of α-endosulfan. Spectroscopic measurements were carried out in the region 700–300 nm in potassium phosphate buffer (1 mM, pH = 6.5). For standard curve creation, the absorbance at 562 nm was measured (3 min response time for color development).

3.9. Stability analysis of the immobilized enzyme

Stability analysis of the wild-type and its Phe117Ile mutant (free and sol-gel entrapped) at 4 °C was monitored by periodically measurement of enzyme activity in 1 mM potassium phosphate buffer pH 6.5 using the CDNB/GSH system [17].

4. Results and discussion

4.1. The interaction of PvGmGSTUG with pesticides

GSTs that belong to the *tau* class contain a deep binding cleft, which has been evolved to accommodate a broad range of hydrophobic substrates and non-substrate ligands [18,20]. Non-substrate ligands usually bind to the L-site (ligandin-binding site), which is located in a distinct region or overlaps with the G- and H-sites [51,52]. The binding of these compounds to the L-site of GSTs affects the binding of the normal substrates and therefore inhibits the enzyme's catalytic activity [53]. In the present work, the interaction of a wide range of non-substrate ligands (pesticides) with *PvGm*GSTUG was studied to characterize enzyme's binding selectivity towards xenobiotics.

*PvGm*GSTUG is a synthetic isoenzyme that was recently designed and created in our lab [39] by DNA shuffling of abiotic stress-inducible GST genes from *Phaseolus vulgaris* and *Glycine* max. The interaction was investigated by measuring the inhibition of the enzyme's catalytic activity. As shown in Fig. 1, *PvGm*GSTUG displays a wide binding specificity and interacts with a wide range of pesticides. Among all tested compounds, the most potent inhibitors were selected for screening with mutants.

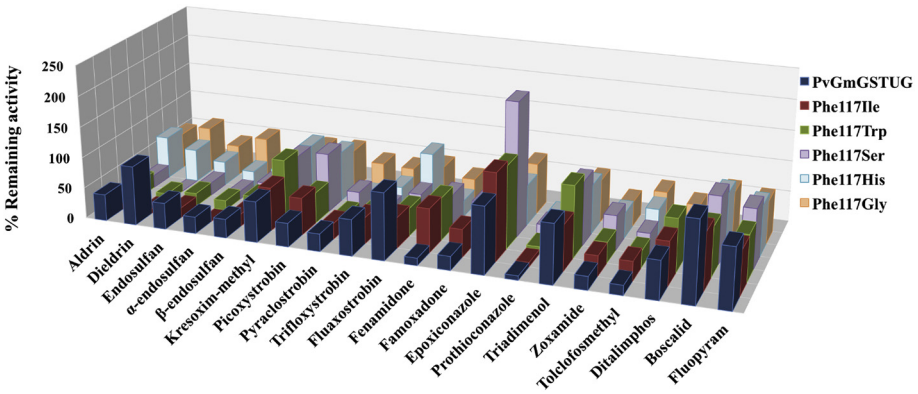

Fig. 1. Inhibition of the wild-type enzyme and the mutants Phe117Ile, Phe117Gly, Phe117His, Phe117Trp, Phe117Ser by pesticides (100 μM). In the absence of pesticides, enzyme activity was taken as 100%. Experiments were performed in triplicate using GSH-CDNB as substrate system.

Table 1
Steady-state kinetic analysis of *PvGm*GSTUG and its mutants for the CDNB/GSH substrate system using as a variable substrate GSH. The CDNB was used at saturated concentration.

Enzyme	K_m (mM) (GSH)	k_{cat} (min^{-1}) (GSH)	k_{cat}/K_m ($mM^{-1}\,min^{-1}$) (GSH)
Wild-type (*PvGm*GSTUG)	1.17 ± 0.090	194.1 ± 4.85	165.89 ± 16.90
Phe117Ser	0.15 ± 0.013	75.65 ± 1.30	511 ± 53.06
Phe117Gly	0.89 ± 0.09	60.16 ± 2.49	67.60 ± 9.63
Phe117His	0.38 ± 0.038	69.44 ± 1.76	182.73 ± 22.90
Phe117Trp	0.57 ± 0.06	194 ± 6.13	340.35 ± 46.58
Phe117Ile	0.22 ± 0.024	116.6 ± 2.80	530.0 ± 70.54

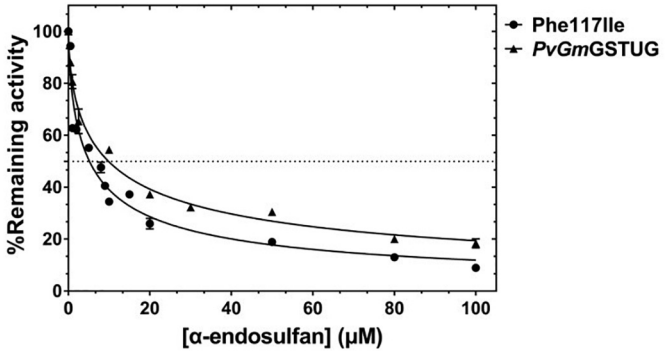

Fig. 2. Dose-response inhibition effect of α-endosulfan on the wild-type *PvGm*GSTUG (▲) (IC_{50} value: 9.84 ± 0.61 μM) and mutant Phe117Ile (●) (IC_{50} value: 5.17 ± 0.47 μM) enzymes. GSTs were assayed using the CDNB–GSH assay system and the experiments were performed in triplicate.

4.2. Structural determinants that affect pesticide binding to PvGmGST and design of H-site mutants: the role of Phe117

Enzyme-based biosensors that rely on the inhibition of the enzyme activity by xenobiotic compounds, allow their measurement based on the determination of the inhibition of the substrate turnover rates [5,21,26]. Although the enzyme-based biosensors are in general appropriate and efficient, their sensitivity and specificity depend on the enzyme's itself catalytic properties [24]. A suitable enzyme that recognize with high affinity the target compound is a requirement [54]. Protein engineering is, therefore, a powerful strategy for the design of tailor made enzymes with appropriate improvements for the development of such analytical applications [55].

Analysis of the molecular model of *PvGm*GSTUG revealed that Phe117 seems to be in a rather remote end of the *PvGm*GSTUG structure without too much involvement in the overall fold of the enzyme. However, careful study and exhaustive molecular dynamics simulation prove that Phe117 is a key residue and plays a central role in binding and catalysis. Phe117 is strategically located immediately after helix H4 and just before helix H5. It establishes interactions with a set of positively charged residues nearby. Namely, hydrogen bonds and π-stacking interactions are formed between Phe117, the preceding Arg113 and the following Lys122 and Arg124 residues (Fig. 3) That interaction arrangement is pivotal and vital for the spatial arrangement of the H4 helix. Disruption of these interactions results in a rather significant change in the relative angle between helices H4 and H6 with a potentially profound effect to the H-site. The evolutionary study revealed that the closest GST structure bearing GSH is the 2CA8 PDB file (Suppl. Fig. 1). The two structures were superimposed and the GSH coordinates were copied to the *PvGm*GSTUG molecular system. The system was energetically optimized and subjected to molecular dynamics simulations. The interaction pattern revealed a stabilizing mechanism for the *PvGm*GSTUG enzyme that is highly dependent on position 117. In more detail, as mentioned above, the H4 helix is spatially coordinated by the loop bearing the 117 position. The H4 helix is stabilized by hydrogen bonding of Asp105 in the midst of the helix to Arg21 (Fig. 4A-B). Consequently, Arg21 hydrogen bonds and stabilizes Phe18, which is a key residue to the GSH coordination and catalysis (Fig. 4C-D). Any change in position 117 will trigger a cascade that will affect significantly the substrate binding and catalysis via the Asp105 → Arg21 → Phe18 route.

Phe117 was subjected to site-saturation mutagenesis aiming at creating a new enzyme variant with improved catalytic and binding properties towards α-endosulfan. Following site-saturation mutagenesis, the coding sequences of the mutant enzymes were cloned, expressed in *E. coli* BL21(DE3) and the library of the mutated enzymes were screened using activity assays [56] for selecting mutant enzymes with high inhibition potency towards α-endosulfan. Five clones displaying the desired characteristics were selected for further study. Sequencing analysis verified that the five clones contained a single point mutation at position 117. The substitutions were amino acids with wide diversity in their physicochemical properties: Ile, His, Trp, Gly and Ser.

4.3. Kinetic analysis of site-saturation enzyme variants

The wild-type *PvGm*GSTUG enzyme and site-saturations variants were purified by affinity chromatography and subjected to steady-state kinetic analysis and the results are shown in Fig. 5 and the kinetic parameters in Table 1 and Table 2. Kinetic analysis using GSH as variable substrate (Table 1) showed that all site-saturation variants obey Michaelis-Menten kinetics and display improved affinity for GSH, compared to the wild-type enzyme. The improvement in K_m^{GSH} value is higher for the mutants Phe117Ile and Phe117Ser (~5-fold) which is translated to 3-fold improvement in catalytic efficiency (k_{cat}/K_m^{GSH}) (Table 1). Kinetic analysis using CDNB as variable substrate (Fig. 5, Table 2), showed that all but Phe117Ser mutant do not obey Michaelis-Menten kinetics, but rather a sigmoid dependence on substrate concentration with Hill coefficient > 1, suggesting a positive cooperativity between the two H-sites.

The role of Phe117 was further investigated by in silico mutagenesis experiments. All mutants were modelled on a computer-based

Table 2
Steady-state kinetic analysis of *PvGm*GSTUG and its mutants for the CDNB/GSH substrate system using as a variable substrate CDNB. The GSH was used at saturated concentration.

Enzyme	$S_{0.5}$ (mM) (CDNB)	k_{cat} (min^{-1}) (CDNB)	n_H (CDNB)	k_{cat}/K_m ($mM^{-1}\,min^{-1}$)
Wild-type (PvGmGSTUG)	0.88 ± 0.05	–	1.77 ± 0.14	–
Phe117Ser	2.59 ± 0.31[a]	97.98 ± 7.15	–	37.83 ± 7.28[b]
Phe117Gly	0.94 ± 0.057	–	2.30 ± 0.23	
Phe117His	0.92 ± 0.07	–	1.50 ± 0.11	
Phe117Trp	0.68 ± 0.05	–	2.09 ± 0.23	
Phe117Ile	0.71 ± 0.07	–	1.33 ± 0.13	

[a] The mutant Phe117Ser enzyme obeys Michaelis-Menden kinetics and this value should be considered as K_m (mM).
[b] The mutant Phe117Ser enzyme obeys Michaelis-Menden kinetics and this value should be considered as k_{cat}/K_m ($mM^{-1}\,min^{-1}$).

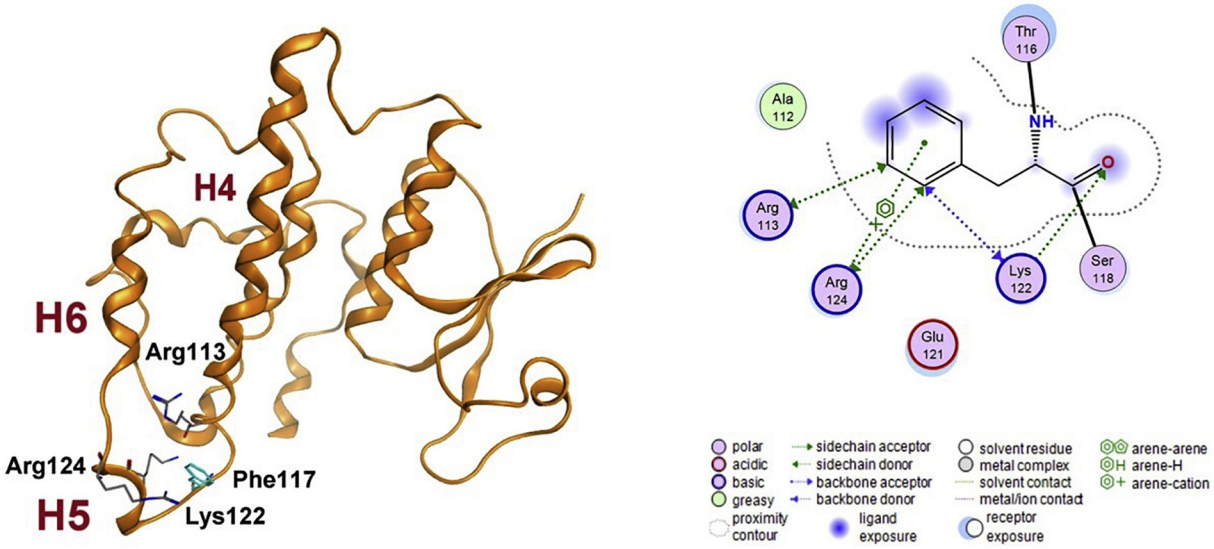

Fig. 3. Study of the structural significance of Phe117 on the fold and function of the *PvGm*GSTUG enzyme. Left: The 3D structure of *PvGm*GSTUG with the Phe117 residue highlighted in turquoise color. The key interacting residues are shown in stick representation. Right: The 2D interaction diagram for the residue Phe117.

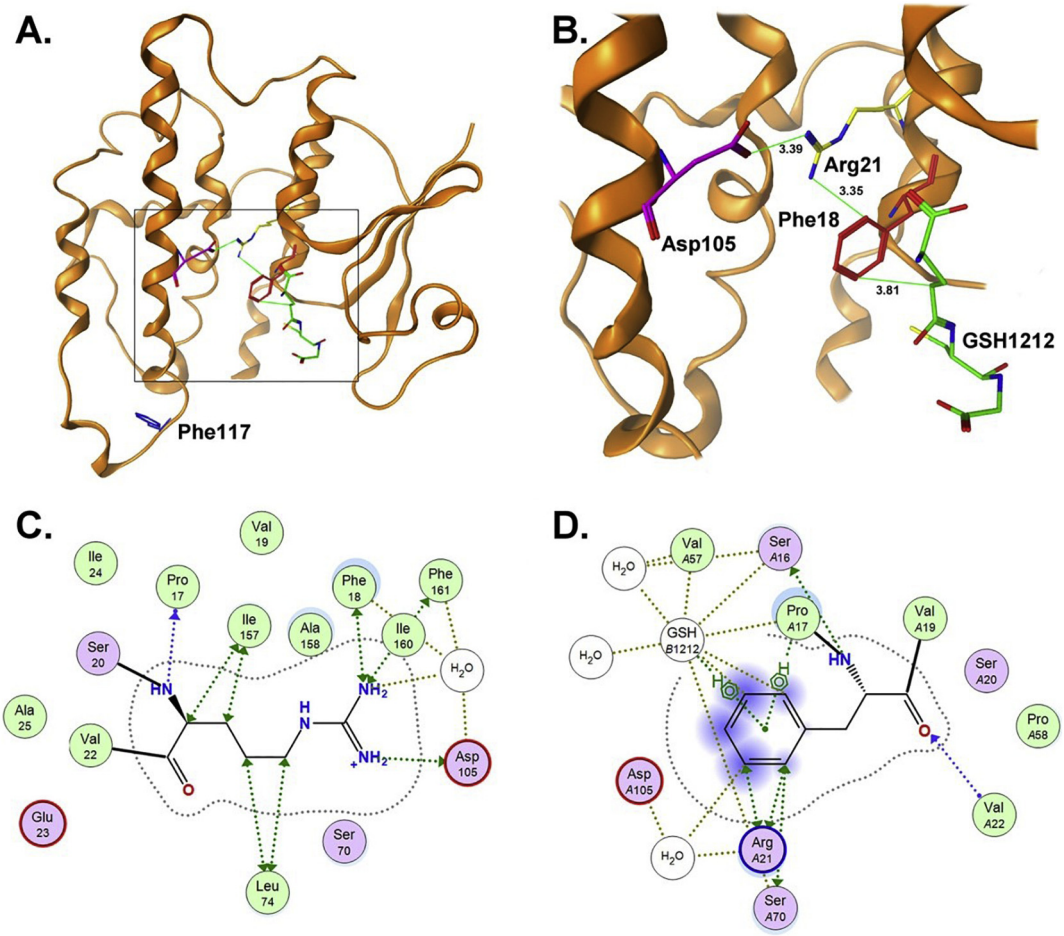

Fig. 4. The structural mechanism that elaborates how the Phe117 residue can influence the catalytic potential of the *PvGm*GSTUG enzyme. A: The structure of the *PvGm*GSTUG enzyme with key residues highlighted in stick representation. B: Zoom-in of A. C: The 2D interaction diagram for the residue Arg21. D: 2D interaction diagram for the residue Phe18.

molecular system and were subjected to unrestrained, explicitly solvated molecular dynamics (MDs) simulations. The results of the molecular modelling study coincide with the experimental results (Tables 1 and 2) and solidify the proposed mechanism described herein. The wild-type enzyme and the Phe117His mutant behave quite similarly as the side chains of the Phe and His residue are capable of establishing the same interactions. The imidazole ring of His residue can maintain the interactions of the original benzene ring of the Phe of the wild-type

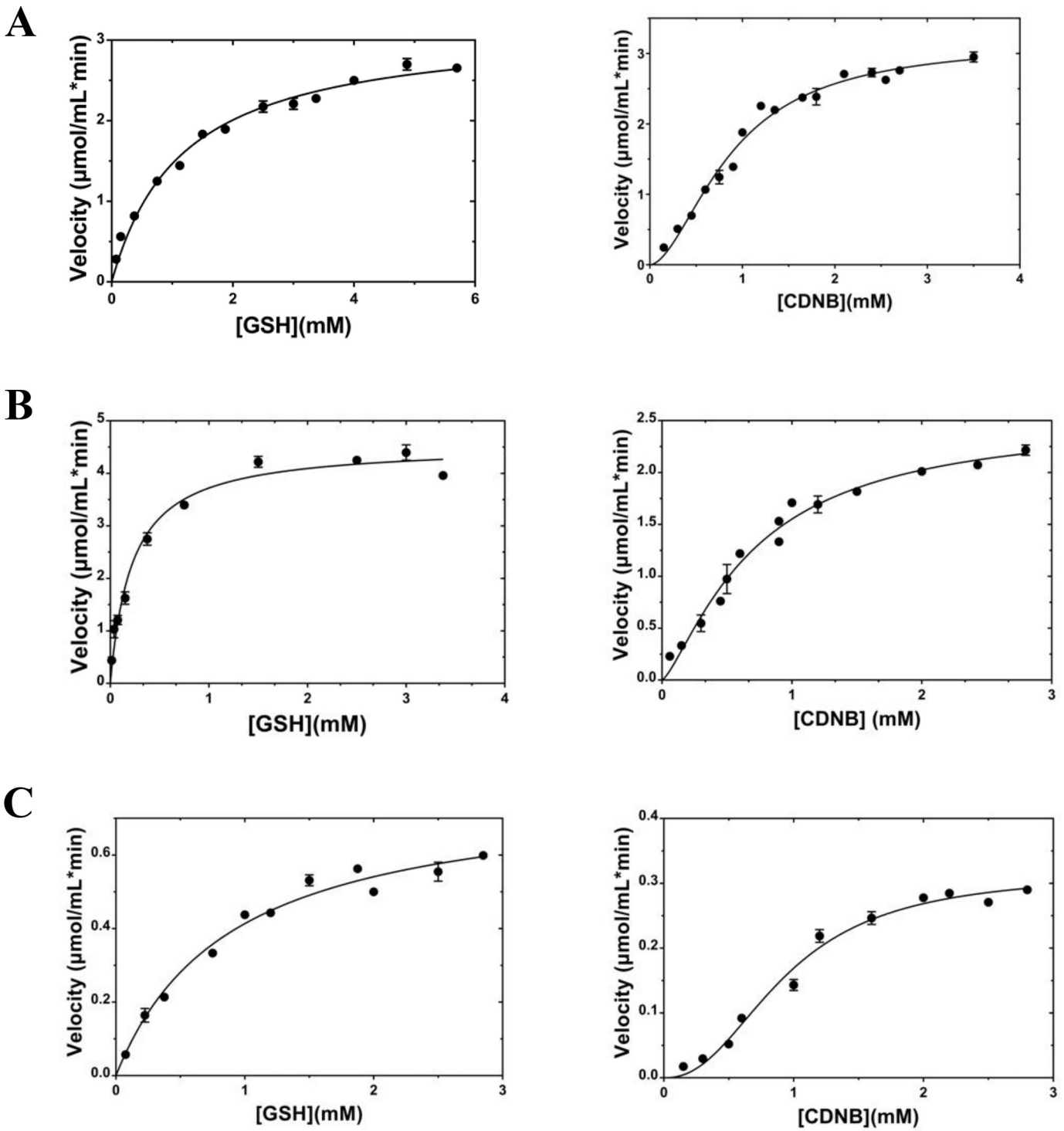

Fig. 5. Kinetic analysis of the wild-type *PvGm*STUG and its mutants (Phe117Ile, Phe117Gly, Phe117His, Phe117Trp and Phe117Ser), using the GSH as a variable substrate and CDNB at a fixed concentration (left graphs) or using the CDNB as a variable substrate and GSH a fixed concentration (right graphs). A: wild-type enzyme *PvGm*STUG, B: mutant Phe117Ile, C: mutant Phe117Gly, D: mutant Phe117His, E: mutant Phe117Trp and F: mutant Phe117Ser.

enzyme. Consequently, the structure of Phe117His mutant remains unchanged upon MDs (Fig. 6C). The structure of Phe117Gly mutant is the only one of the five variants that resulted in a relative shift of the H4 helix towards the catalytic site, thus via the Asp105 to Arg21 interaction pushing Phe18 into the conformational space of the catalytic site and restraining and limiting the spatial flexibility of the ligand (Fig. 6B). On the contrary, the Phe117Ser, Phe117Trp and Phe117Ile variants produced molecular systems where the H4 helix is tilted and slightly shifted away from the catalytic site. This structural effect has consequently dragged Arg21 towards Asp105 and has allowed more space to Phe18. This translates in an increase of the overall volume of the catalytic site. The increase in volume is most observed in the Phe117Ile mutant, with the Phe117Ser to follow and the Phe117Trp mutant with the least increase in the volume of the catalytic site of the enzyme (Fig. 6A, D and E).

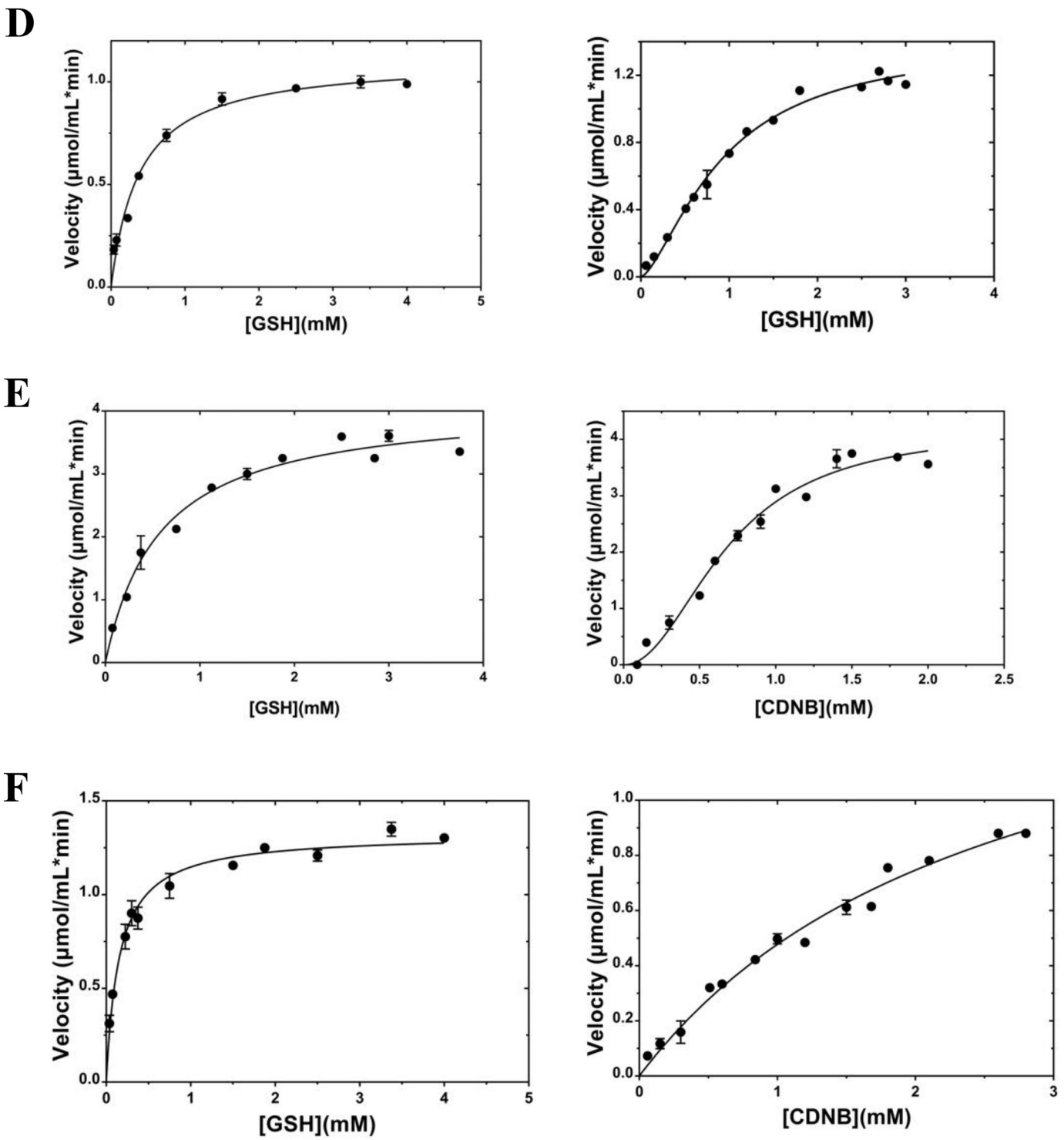

Fig. 5. (*continued*)

4.4. Inhibition analysis of site-saturated enzyme variants towards pesticides

To assess the effect of mutations at position 117 on enzyme's inhibition by pesticides, kinetic inhibition analysis was carried out (Fig. 1). The results showed that the mutants Phe117Ile, Phe117Trp, and Phe117Ser display higher sensitivity towards organochloride insecticides. Among all mutants, Phe117Ile was more sensitive towards α-endosulfan, reaching 100% inhibition. Concentration-response curves (Fig. 2), for the wild-type enzyme and the mutant Phe117Ile, showed that the latter enzyme is more sensitive to inhibition by α-endosulfan (IC_{50} = 5.17 ± 0.47 μM) compared to the wild-type enzyme (9.836 ± 0.610 μM) (Fig. 2). The ability of α-endosulfan to bind and inhibit the catalytic activity of mutant Phe117Ile was explored for the development of analytical enzyme-based biosensor.

In an effort to investigate in silico the binding potential of the Phe117Ile mutant, α-endosulfan was docked and the resulting molecular system was subjected to MDs alongside the same system of the wild-type enzyme. The systems reached equilibrium and the molecular interactions of the docked α-endosulfan compound were identified (Fig. 7). The results confirm that the Phe117Ile mutant has a rather

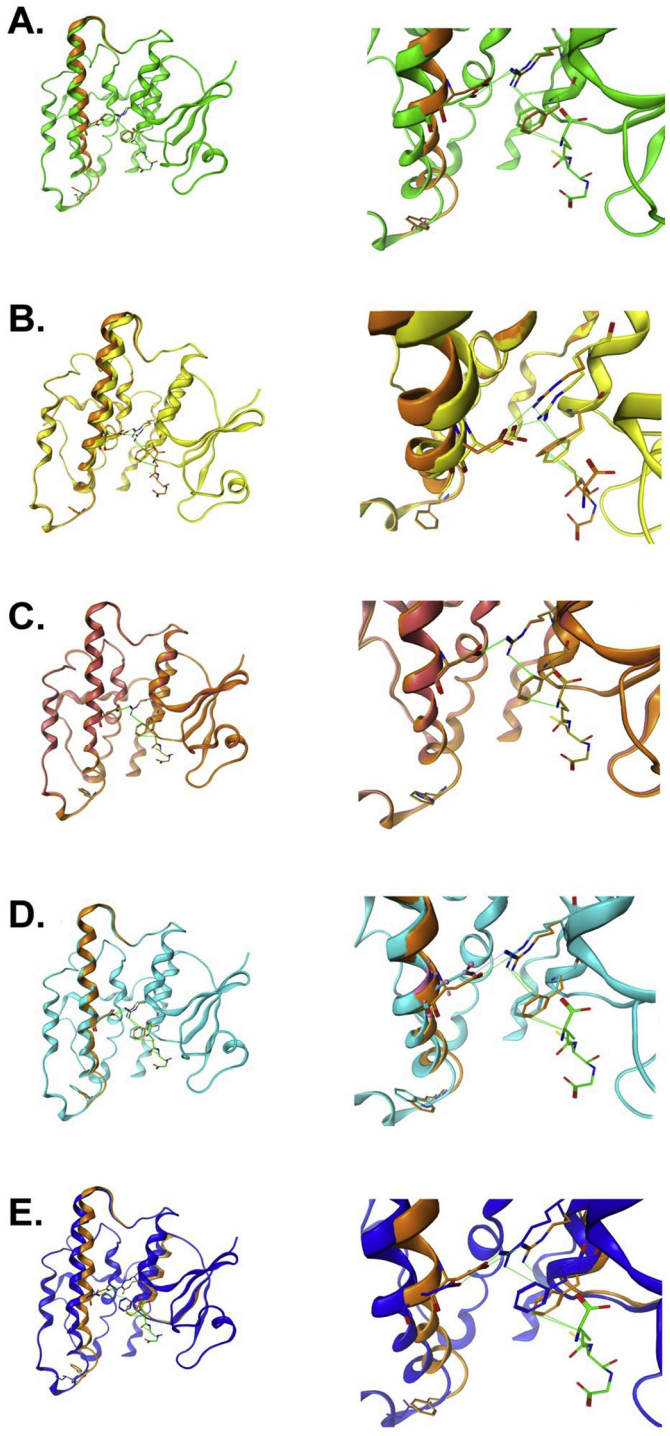

Fig. 6. In silico mutation study for the *PvGm*GSTUG mutants A: Phe117Ser, B: Phe117Gly, C: Phe117His, D: Phe117Trp and E: Phe117Ile.

larger catalytic site (> 25% increase in volume) when compared to the wild-type enzyme. Phe18 interacts with α-endosulfan and acts as a barrier that balances α-endosulfan to achieve the two hydrogen bonds with Lys56 and Val57. However, on the Phe117Ile mutant and due to the increase in volume of the catalytic site, the Phe18 residue has moved away, dragged from the movement of the H4 helix, as discussed above. This allowed α-endosulfan to move deeper towards the enzyme core and establish two more interactions with Phe43 and Met13. This shift does not only allow the extra two interactions but more importantly it coordinates α-endosulfan in optimal position for Lys56 to interact with the -S=O moiety and secure higher affinity of the Phe117Ile mutant for this compound, when compared to the wild-type enzyme.

4.5. Enzyme immobilization, stability and kinetic analysis

The mutant enzyme Phe117Ile was entrapped in a sol-gel polymer (Fig. 8), which was synthesized by condensation reaction between TEOS and PTMOS at acidic pH in the presence of CTAB, a single chained cationic surfactant [9,15]. Leaching of the enzyme through diffusion from the sol-gel matrix was not detected. The use of CTAB allows the synthesis of a flexible silica sol-gel matrix able to adopt suitable shape with desirable pore size network [57] and mechanical strength [58]. The use of alkoxysilane, PTMOS and TEOS are preferred for enzyme immobilization due to their ability to provide desirable pore structure, uniform pore-size distribution, high specific pore volumes, large internal surface area [59] and surface functionalities [60].

After sol-gel synthesis, “aging” of the matrix was achieved for two or five days. During the “aging” process, cross-linking of the polymer network increases and the internal solvent is expelled from the matrix, causing alterations in internal polarity and viscosity. In addition, the average pore size decreases [61]. This “aging” step was found to be crucial, as resulted in improvement in enzyme stability, as illustrated in Fig. 9. As it can be seen from the figure, the activity of the entrapped enzyme decreased at a significant lower rate, compared to that of the free enzyme under the same conditions. The immobilized enzyme retained > 60% of its initial activity after about twenty-five days, while the free enzyme totally lost its activity after twelve days of storage. These data clearly show that the entrapment benefited significantly the long-term stability of the enzyme, which improves considerably the practical viability of this system.

The concentration–response curve of the entrapped enzyme for α-endosulfan was assessed and the results are shown in Fig. 10. As can be seen from the figure, the entrapped enzyme notably retains its sensitivity towards α-endosulfan but exhibits increased affinity with an IC_{50} of 2.60 ± 0.22 μM, suggesting that the sol-gel process provides an appropriate technology for the development of a GST-based biosensor.

4.6. Biosensor assessment and application

The sensing-signal of the GST-based biosensor exploited the inhibition by α-endosulfan of the CDNB/GSH conjugation reaction, catalysed by the sol-gel entrapped mutant Phe117Ile.

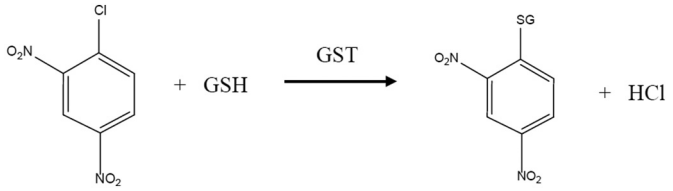

The concentration of released H^+ ions reflects the progress of the conjugation reaction and therefore pH, changes can be transduced to an optically measurable signal by the immobilized indicators. The mixture of bromocresol purple and phenol red provided adequate sensitivity and reproducibility. Fig. 11A shows the VIS spectrum of sol–gel entrapped mixture of two dyes at pH values ranging from 4.0 to 7.0. As can be seen, the mixture of the two indicators exhibits two distinct absorption maxima, at 444 and 562 nm. Linear dependence (R^2 = 0.98) of the absorption at 562 nm versus pH was found between pH 4 to 7 (Fig. 11B). The optical signal at 562 nm of the sol-gel entrapped Phe117Ile mutant enzyme was assessed using different concentrations of α-endosulfan (Fig.11C). As can be seen in Fig. 11D a linear dependence (R^2 = 0.98) of the absorption at 562 nm versus different concentrations of α-endosulfan (0.625–30 μM) was observed, suggesting that the system can provide a high sensitive analytical method for α-

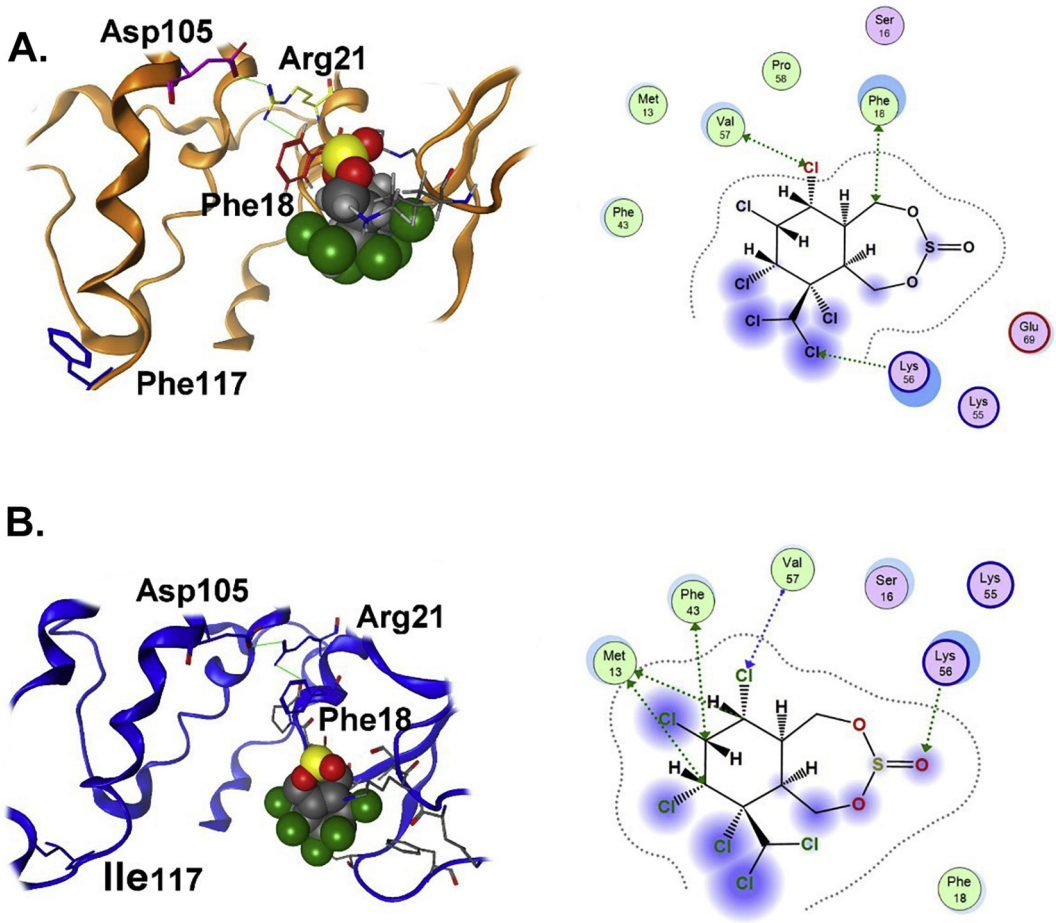

Fig. 7. Molecular docking of α-endosulphan in the *PvGm*GSTUG structure. A: The wild type *PvGm*GSTUG with docked α-endosulphan. B: The Phe117Ile mutant *PvGm*GSTUG with docked α-endosulphan.

endosulfan determination.

The biosensor was further evaluated using real water samples (finished drinking water and bottled mineral water) spiked with known concentrations of α-endosulfan and the results are illustrated in Fig. 12. The optical signal at 562 nm obeys different response when used drinking water and mineral water, compared to that observed using ddH_2O. This may be due to the differences in salt and organic content of the two water samples. Linearity was observed within the concentration range of 0.8–16 μM of α-endosulfan, obeying the following equations:

Mineral water: $y = 0.0249\times + 0.338$, ($R^2 = 0.99$)

Drinking water: $y = 0.0472\ x + 0.303$, ($R^2 = 0.99$)

Recovery experiments using drinking water and bottled mineral water samples spiked with a known amount of α-endosulfan, were also achieved and the results are listed in Table 3. Recoveries of α-endosulfan in the mineral water were in the range between 80.6 and 103% (mean value 93.42 ± 3.25%, $N = 6$). For drinking water, recoveries were ranged between 88 and 104% (mean value 98.6 ± 3.46%, N = 4). The reproducibility of the assay response, expressed by relative standard deviation, was in the order of 8.54% and 7.02% for the mineral and drinking water, respectively.

The design of enzyme biosensors is mainly based on the knowledge about the target analyte, as well as the complexity of the biological sample as well as the matrix in which the analyte has to be determined. The application of enzymes with wide binding specificity for developing biosensors, such as acetylcholinesterases [63–65], tyrosinases [66] and GSTs [3,9,17,22–26], suffer from poor specificity since many inhibitors can interfere and therefore one limitation of such biosensors is the difficulty in discriminating between different inhibitors. Such biosensors can only be used for the quantification of a known analyte (e.g. α-endosulfan in the present work) in a sample where only this particular known analyte is present. Alternatively, such biosensors can be exploited as detection systems able to detect several analytes simultaneously. This can be achieved using data processing of Artificial Neural Networks (ANNs) coupled with a sensor array. This combination can substantially improve the selectivity and allow exact determination of pesticides present in a sample. ANN can combines the response of different enzymes (e.g. different engineered forms of GST) to find a pattern that relates inhibitor concentrations with the inhibition percentages measured. Such biosensors have been developed based on acetylocholinesterase [63–65] or tyrosinase [66] inhibition and chemometric data analysis using ANNs. This area represents a very promising approach in environmental monitoring and screening.

5. Conclusion

In the present work, a structure-based combinational approach was used for the design of an optimized mutant of *PvGm*GSTUG, for the development of an optical biosensor for α-endosulfan determination. Site-saturation mutagenesis at residue 117 proved to be a successful approach for the improvement of enzyme's sensitivity towards α-endosulfan. The proposed biosensor provides a low-cost alternative to current chromatographic-based methods [62]. Since GSTs exhibit wide inhibition capabilities, the present approach can be further adapted and optimized to different pesticides, providing a route for developing analytical tools for environmental and toxicological applications.

Supplementary data to this article can be found online at https://doi.org/10.1016/j.bbagen.2018.12.004.

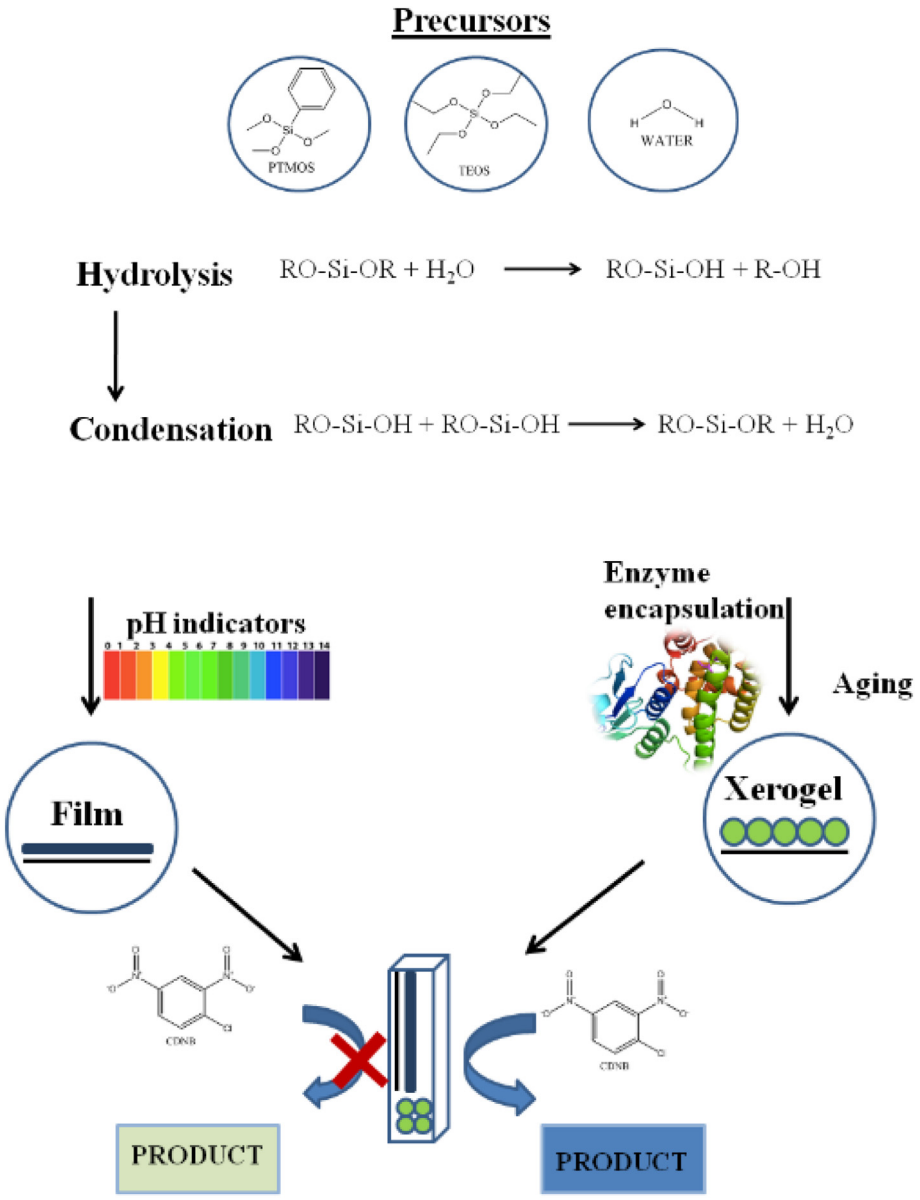

Fig. 8. Schematic illustration of the GST -based biosensor system for the determination of α-endosulfan.

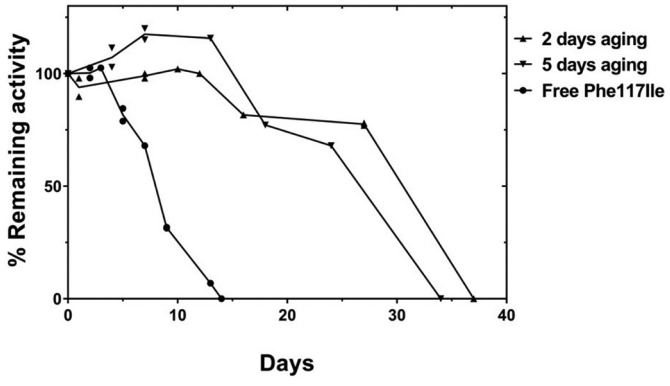

Fig. 9. Stability analysis of the free and the entrapped mutant enzyme Phe117Ile. The effect of gel aging (2 and 5 days) on the stability was also investigated.

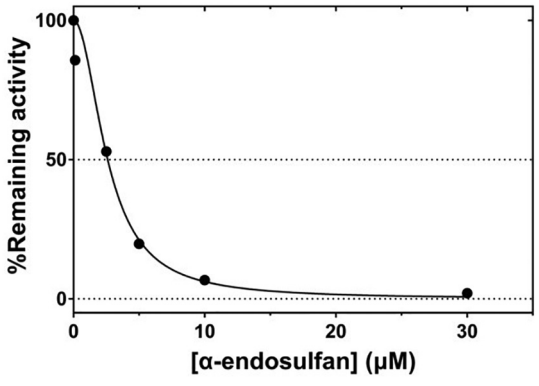

Fig. 10. Dose-response inhibition of α-endosulfan on the sol-gel entrapped Phe117Ile mutant enzyme. All assays were accomplished using the CDNB–GSH assay system and the experiments were performed in duplicate.

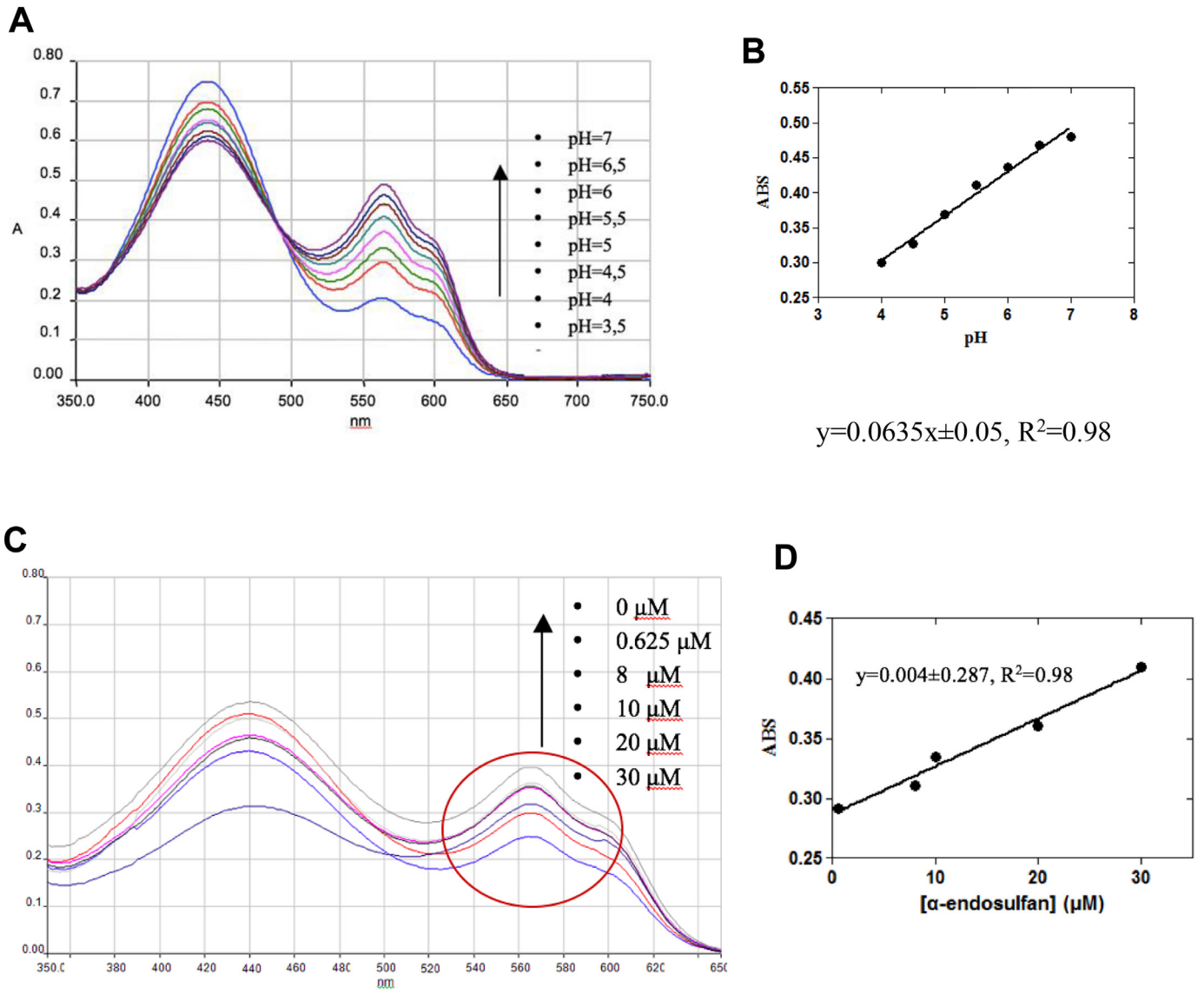

Fig. 11. Dependence of optical signal on pH. A. Visible spectra of sol–gel with entrapped bromocresol purple/phenol red at different pH values B. Calibration curve of the absorption at 562 nm on different pH. C. Visible spectra of the sol-gel co-entrapped Phe117Ile and bromocresol purple/phenol red in the presence of different concentration of α-endosulfan (0–30 μM). D: Calibration curve of the absorbance at 562 nm on α-endosulfan concentration (0–30 μM).

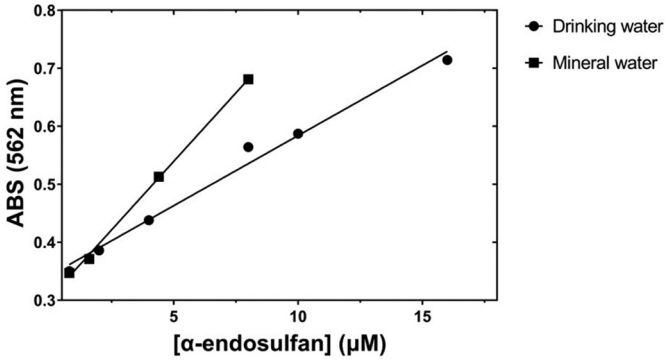

Fig. 12. Dependence of the absorbance at 562 nm on α-endosulfan concentration (0–30 μM) using drinking (●) and mineral (■) water.

Table 3
Pesticide recovery experiments in water samples spiked with known amounts of α-endosulfan.

Sample	Added (μM)	Control	Spiked	Recovery (%)
Mineral water	0.8	0.34	0.35	102.9
	2	0.41	0.38	94.2
	4	0.5	0.44	87.6
	8	0.55	0.56	102.7
	10	0.7	0.58	83.9
	16	0.8	0.71	89.3
RSD[a] (%)				8.54
Drinking water	0.8	0.33	0.35	104.5
	1.6	0.42	0.37	88.8
	4	0.50	0.51	102.2
	8	0.68	0.68	98.9
RSD[a] (%)				7.02

[a] RSD: relative standard deviation.

Conflict of interest

None to declare.

Acknowledgement

NEL and FSA acknowledge the International Scientific Partnership Program at King Saud University, Saudi Arabia, for funding this research work through ISPP# 0071.

References

[1] A.J. Dowd, A. Steven, E. Morou, J. Hemingway, J. Vontas, M.J.I. Paine, Enzym. Microb. Technol. 45 (2009) 164.
[2] K. Kiilerich-Hansen, C.R. Poulsen, J. Daprà, O. Nikolaj, C. Rozlosnik, N. Rozlosnik, Polymer based biosensors for pathogen diagnostics, in: V. Somerset (Ed.), Environmental Biosensors, IntechOpen, 2011, pp. 193–209.
[3] E. Morou, H.M. Ismail, A.J. Dowd, J. Hemingway, N. Labrou, M. Paine, J. Vontas, Anal. Biochem. 378 (2008) 60.
[4] G. Rocchitta, A. Spanu, S. Babudieri, G. Latte, G. Madeddu, G. Galleri, S. Nuvoli, P. Bagella, M.I. Demartis, V. Fiore, R. Manetti, P.A. Serra, Sensors 16 (2016) 780.
[5] A. Sassolas, L.J. Blum, B.D. Leca-Bouvier, Biotechnol. Adv. 30 (2012) 489.
[6] B. Bucur, F.-D. Munteanu, J.-L. Marty, A. Vasilescu, Biosensors (Basel) 8 (2018) 27.
[7] A. Amine, F. Arduini, D. Moscone, G. Palleschib, Biosens. Bioelectron. 76 (2016) 180.
[8] M. Trojanowicz, Electroanalysis 14 (2002) 1311.
[9] V.G. Andreou, Y.D. Clonis, Anal. Chim. Acta 460 (2002) 151.
[10] S. Andreescu, A. Avramescu, C. Bala, V. Magearu, J.L. Marty, Anal. Bioanal. Chem. 374 (2002) 39.
[11] K. Flavin, J. Mullowney, B. Murphy, E. Owens, P. Kirwan, K. Murphy, H. Hughes, P. McLoughlin, Analyst 132 (2007) 224.
[12] C. Kascholke, S. Hendrikx, T. Flath, D. Kuzmenka, H.M. Dörfler, D. Schumann, M. Gressenbuch, F.P. Schulze, M. Schulz-Siegmund, M.C. Hacker, Acta Biomater. 63 (2017) 336.
[13] A. Kloskowski, M. Pilarczyk, W. Chrzanowski, J. Namieśnikournal, Crit. Rev. Anal. Chem. 40 (2010) 172.
[14] A.E. Danks, S.R. Hall, Z. Schnepp, Mater. Horiz. 3 (2016) 91.
[15] R. Gupta, N.K. Chaudhury, Biosens. Bioelectron. 22 (2007) 2387.
[16] N. Allocati, L. Federici, M. Masulli, C. Di Ilio, FEBS J. 276 (2009) 58.
[17] E. Chronopoulou, A.C. Papageorgiou, A. Markoglou, N.E. Labrou, J. Mol. Cat. B: Enzymatic. 81 (2012) 43.
[18] B. Mannervik, U.H. Danielson, CRC Crit. Rev. Biochem. 23 (1988) 283.
[19] J.D. Hayes, J.U. Flanagan, I.R. Jowsey, Annu. Rev. Pharmacol. Toxicol. 45 (2005) 51.
[20] D. Sheehan, G. Meade, V.M. Foley, C.A. Dowd, Biochem. J. 360 (2001) 1.
[21] E. Chronopoulou, P. Madesis, B. Asimakopoulou, D. Platis, A. Tsaftaris, N.E. Labrou, Planta 235 (2012) 1253.
[22] J.W. Choi, Y.K. Kim, S.Y. Song, I.H. Lee, W.H. Lee, Biosens. Bioelectron. 18 (2003) 1461.
[23] E.G. Chronopoulou, N.E. Labrou, Recent Pat. Biotechnol. 3 (2009) 211.
[24] P. Kapoli, I.A. Axarli, D. Platis, M. Fragoulaki, M. Paine, J. Hemingway, J. Vontas, N.E. Labrou, Biosens. Bioelectron. 24 (2008) 498.
[25] E.M. Materon, P.J. Jimmy Huang, A. Wong, A.A. Pupim Ferreira, P. Sotomayor Mdel, J. Liu, Biosens. Bioelectron. 58 (2014) 232.
[26] T.I. Oliveira, M. Oliveira, S. Viswanathan, M. Fátima Barroso, L. Barreiros, O.C. Nunes, J.A. Rodrigues, P. de Lima-Neto, S.E. Mazzetto, S. Morais, C. Delerue-Matos, Talanta 106 (2013) 249.
[27] V. Tiwari, Front. Chem. 4 (2016) 39.
[28] C. Bernal, K. Rodriguez, R. Martínez, Biotechnol. Adv. 36 (2018) 1470.
[29] K. Tars, B. Olin, B. Mannervik, J. Mol. Biol. 397 (2010) 332.
[30] Y. Ivarsson, A.J. Mackey, M. Edalat, W.R. Pearson, B. Mannervik, J. Biol. Chem. 278 (2003) 8733.
[31] M.A. Norrgård, B. Mannervik, J. Mol. Biol. 412 (2011) 111.
[32] N.E. Labrou, M.M. Muharram, M.S. Abdelkader, Biochim. Biophys. Acta 1864 (2016) 1315.
[33] J. Damborsky, J. Brezovsky, Curr. Opin. Chem. Biol. 19 (2014) 8.
[34] S. Lutz, Curr. Opin. Biotechnol. 21 (2010) 734.
[35] R. Verma, U. Schwaneberg, D. Roccatano, Comput. Struct. Biotechnol. J. 2 (2012) e201209008.
[36] M. Bilal, H.M.N. Iqbal, S. Guo, H. Hu, W. Wang, X. Zhang, Int. J. Biol. Macromol. 108 (2018) 893.
[37] J. Weber, C.J. Halsall, D. Muir, C. Teixeira, J. Small, K. Solomon, M. Hermanson, H. Hung, T. Bidleman, Sci. Total Environ. 408 (2010) 2966.
[38] M. Bradford, Anal. Biochem. 72 (1976) 248.
[39] E.G. Chronopoulou, A.C. Papageorgiou, F. Ataya, I. Nianiou-Obeidat, P. Madesis, N.E. Labrou, Front. Plant Sci. 9 (2018) 737, https://doi.org/10.3389/fpls.2018.01737.
[40] M. Magrane, Uniprot Consortium, Database, 2011 (2011) bar009.
[41] D.A. Benson, I. Karsch-Mizrachi, D.J. Lipman, J. Ostell, E.W. Sayers, Nucleic Acids Res. 39 (2011) D32.
[42] S.F. Altschul, W. Gish, W. Miller, E.W. Myers, D.J. Lipman, J. Mol. Biol. 215 (1990) 403.
[43] C.J. Sigrist, E. de Castro, L. Cerutti, B.A. Cuche, N. Hulo, A. Bridge, L. Bougueleret, I. Xenarios, Nucleic Acids Res. 41 (2013) D344.
[44] J.D. Thompson, D.G. Higgins, T.J. Gibson, Nucleic Acids Res. 22 (1994) 4673.
[45] J. Castresana, Mol. Biol. Evol. 17 (2000) 540.
[46] D.T. Jones, W.R. Taylor, J.M. Thornton, Comput. Appl. Biosci. 8 (1992) 275.
[47] D.H. Huson, D.C. Richter, C. Rausch, T. Dezulian, M. Franz, R. Rupp, BMC Bioinformatics 8 (2007) 460.
[48] R. Chen, L. Li, Z. Weng, Proteins 52 (2003) 80.
[49] B. Hess, C. Kutzner, D. van der Spoel, E. Lindahl, J. Chem. Theory Comput. 4 (2008) 435.
[50] D. Sellis, D. Vlachakis, M. Vlassi, Bioinform. Biol. Insights 3 (2009) 99.
[51] I. Axarli, P. Dhavala, A.C. Papageorgiou, N.E. Labrou, J. Mol. Biol. 385 (2009) 984.
[52] P. Reinemer, L. Prade, P. Hof, T. Neuefeind, R. Huber, R. Zettl, K. Palme, J. Schell, I. Koelln, H.D. Bartunik, B. Bieseler, J. Mol. Biol. 255 (1996) 289.
[53] I.A. Axarli, D.J. Rigden, N.E. Labrou, Biochem. J. 382 (2004) 885.
[54] E.M. Gillam, Clin. Exp. Pharmacol. Physiol. 32 (2005) 147.
[55] R.M. Ferraz, A. Vera, A. Arís, A. Villaverde, Microb. Cell Factories 5 (2006) 15.
[56] I. Axarli, A.W. Muleta, E.G. Chronopoulou, A.C. Papageorgiou, N.E. Labrou, Biochim. Biophys. Acta, Gen. Subj. 1861 (2017) 3416.
[57] C. Rottman, G. Grader, Y. De Hazan, S. Melchior, D. Avnir, J. Am. Chem. Soc. 121 (1999) 8533.
[58] B. Wang, B. Li, Q. Deng, S. Dong, Anal. Chem. 70 (1998) 3170.
[59] M. Hartmann, X. Kostrov, Chem. Soc. Rev. 42 (2013) 6277.
[60] A.C. Pierre, Biocatal. Biotransform. 22 (2004) 145.
[61] B. Dunn, J.I. Zink, Chem. Mater. 9 (1997) 2280.
[62] T. Siddique, Z.A. Zahir, W.T. Frankenberger Jr., J. Liq. Chromatogr. Relat. Technol. 26 (2003) 1069.
[63] M. Cortina-Puig, G. Istamboulie, T. Noguer, J.L. Marty, Analysis of pesticide mixtures using intelligent biosensors, in: V.S. Somerset (Ed.), Intelligent and Biosensors, 2010, p. 205.
[64] G. Istamboulie, M. Cortina-Puig, J.L. Marty, T. Noguer, Talanta 79 (2009) 507.
[65] K. Mwila, M.H. Burton, J.S. Van Dyk, B.I. Pletschke, Environ. Monit. Assess. 185 (2013) 2315.
[66] X. Cetó, F. Céspedes, M. del Valle, Talanta 99 (2012) 544.